ISSN 0362-1197, Human Physiology, 2017, Vol. 43, No. 5, pp. 501–511. © Pleiades Publishing, Inc., 2017.
Original Russian Text © A.A. Frolov, G.A. Aziatskaya, P.D. Bobrov, R.Kh. Luykmanov, I.R. Fedotova, D. Húsek, V. Snašel, 2017, published in Fiziologiya Cheloveka, 2017, Vol. 43, No. 5, pp. 17–28.

Electrophysiological Brain Activity during the Control of a Motor Imagery-Based Brain–Computer Interface

A. A. Frolov[a, b, e, *], G. A. Aziatskaya[c], P. D. Bobrov[a, b], R. Kh. Luykmanov[a, c], I. R. Fedotova[b], D. Húsek[d], and V. Snašel[e]

[a] *Pirogov Russian National Research Medical University, Moscow, Russia*
[b] *Institute of Higher Nervous Activity and Neurophysiology, Russian Academy of Sciences, Moscow, Russia*
[c] *Research Center of Neurology, Russian Academy of Sciences, Moscow, Russia*
[d] *Institute of Informatics, Academy of Sciences of the Czech Republic, Prague, Czech Republic*
[e] *Ostrava Technical University, Ostrava, Czech Republic*
**e-mail: aafrolov@mail.ru*

Received April 14, 2017

Abstract—This article considers the features of five electroencephalogram patterns that are most frequently extracted by the independent component analysis when subjects imagine the movement of their hands during the control of a brain–computer interface (BCI). The solution of the EEG inverse problem using the individual geometrical head model shows that the sources of the revealed patterns are located at the bottom of the left and right central sulci, as well as in the left premotor cortex, supplementary motor area, and precuneus. The functional value of the patterns is discussed by comparing the location results with the results of the metaanalysis of the published data that were obtained using a functional magnetic resonance imaging. The source locations are the same for seven healthy subjects and four poststroke patients with subcortical damage location. However, despite the same locations, the two groups of subjects significantly differed in the frequency characteristics of the revealed patterns; in particular, the patients had no clearly pronounced activity in the upper α-band and were characterized by a much lower level of inhibition of rates in the primary somatosensory areas during motor imagery.

Keywords: brain–computer interface, neurointerface, EEG, motor imagery, EEG rhythm synchronization and desynchronization, independent component analysis, EEG inverse problem, neurorehabilitation

DOI: 10.1134/S036211971705005X

The brain–computer interface (BCI) is a hardware-and-software system of a direct interface between the human brain and an external technical device. There are many types of BCIs that are based on the use of different neurophysiological phenomena. One of the most popular types comprises BCIs that are based on the recognition of brain activity patterns that correspond to the imagery of different movements. Today, BCIs are also widely used in theoretical studies on the organization of purposive movements and in clinical practice for substituting or recovering motor functions that were lost after brain damage. Several controlled clinical studies that confirm the BCI effectiveness in neurorehabilitation have already been carried out [1–4].

This article presents the description and analysis of brain activity during the kinesthetic imagery of movements for healthy subjects and poststroke patients with the subcortical location of the damage. The basic tool for analysis of electrophysiological brain activity that is used in our studies is the independent component analysis (ICA); owing to the studies of the group headed by Makeig [5, 6], this method is increasingly more often used for the EEG analysis in general and for the analysis of the data that were obtained during BCI studies in particular [7]. With respect to the EEG analysis, the ICA is based on the generally accepted concept, according to which the electric potential that is recorded on the head surface is superposition of potentials generated by separate discrete sources that are distributed over a large brain volume; each of these sources can be adequately considered as a current dipole. Its activity is characterized by the distribution of electric potential that is generated on the head surface, which is called a topographic map, and by the value of the dipole moment, which sets the current value of its activity. The topographic map of the source depends on the position and orientation of the current dipole within the brain, which can be found by solving the EEG inverse problem. The combination of the ICA and solution of the EEG inverse problem can provide the spatial resolution for the location of inde-

pendent EEG sources that is comparable with the resolution of a functional magnetic resonance imaging (fMRI). According to the authors of the study [6], this will make it possible to return EEG to the forefront of brain imaging.

This article describes and analyzes EEG sources the activity of which was most frequently found on the basis of the ICA during the processing of the data that were recorded from the motor imagery-based BCI study. The locations of the sources are compared with the locations of the hemodynamic activity foci that we determined in [8].

METHODS

The study involved seven male right-handers at the age from 22 to 35 years without clear neurological or psychic disturbances and four poststroke patients at the age from 41 to 60 years with a poststroke period of 1 to 10 months, who had rehabilitation procedures at the Research Center of Neurology in the framework of the iMove multicenter study [2] for assessing the clinical effectiveness of a hand exoskeleton controlled by a brain–computer interface (BCI). The subjects were preliminarily provided with the experimental protocol and gave a written consent for participation in the experiment. The protocol was approved by the Ethics Committee of the Institute of Higher Nervous Activity and Neurophysiology of the Russian Academy of Sciences for healthy subjects and by the Ethics Committee of the Research Center of Neurology for patients.

Experimental procedure. Each subject had 20 experimental BCI control training sessions, two to three sessions per day. The interval between the experimental days was one to four days. All the subjects were instructed to imagine movements on the basis of kinesthetic rather than visual perceptions. The subjects were to perform three instructions that were displayed on a computer screen, namely, to relax or imagine the opening of the left or right hand. Each instruction was displayed for 10 s. Two instructions for the left hand and two for the right hand, which were randomly displayed with the relaxation period that was always preceded by each of them, constituted a block. Each session included five such blocks. The instruction display protocol is described in more detail in [2].

The BCI was controlled using the Bayessian classifier described in [9]. The classifier was trained for recognizing the imagery of the opening of the left or right hand, as well as the relaxation state, according to the data of the first block, and was then additionally trained after each new block. The biofeedback that informed the subjects on the quality of the performance of the mental task provided by the instruction was carried out on the basis of changes in the brightness of the central circle on the computer screen, depending on the probability of the recognition of the EEG pattern that corresponded to the instruction. In addition, the biofeedback in the patients was simultaneously performed on the basis of hand opening using an exoskeleton. The rate of opening was also proportional to the probability of the correct recognition of an EEG pattern that corresponded to the instruction.

The EEG was recorded using a Neirovizor BMM-52 encephalograph (Medical Computer Systems, Russia) with 32 AgCl electrodes. The sampling rate was 500 Hz.

Before EEG was decomposed into independent components, all recordings were successively filtered using a filter that suppressed 50 Hz power-supply noise and a filter with a frequency band of 5 to 30 Hz. An algorithm of bidirectional filtration was used for compensating the time delay of each filter.

Processing of EEG recordings using the independent component analysis. In the general case, the decomposition into independent components is a signal in the form of the sum

$$X = w_1\xi_1 + w_2\xi_2 + \ldots w_k\xi_k, \quad (1)$$

where X is an EEG matrix in which the number of lines is equal to the number of recording electrodes and the number of columns corresponds to the number of recorded signal counts; k is the number of determined independent components. Topographically, the map of the ith source is determined by the weight vector w_i and its activity in the course of time is determined by the line ξ_i.

This study used the *AMICA* method to find the sources of electrophysiological brain activity during motor imagery [10]. In this method, the number of independent components is equal to the number of recording electrodes; therefore, in the case under consideration, $k = 32$ in Eq. (1).

The independent components were determined separately for each session and each subject. Therefore, a total of 7040 components were obtained: 32 components for each of the 20 sessions with 11 subjects.

Location of EEG sources. The source was located for each of the determined independent components on the basis of the solution of the EEG inverse problem, with the individual geometry of the brain and its coverings taken into account. The geometrical model was constructed on the basis of images that were obtained in the Research Center of Neurology using a Siemens Magnetom Verio magnetic resonance tomograph (MRT) with a magnetic induction of 3 T. The recording was made in the T_1 regime: TR = 1900 ms, TE = 2.47 ms, 512 × 512 matrix, FOV = 250 × 250 mm, the section thickness was 1 mm, the voxel size = 0.488 × 0.488 × 1 mm. According to the MRT data, a finite element mesh was constructed for each subject, which made it possible to set the electric conductivity distribution over the tissue of the brain and its covers that was required for the calculation of electric potential distribution over the head surface, depending on the

position and orientation of the current dipole that generated this potential. For this purpose, the MRT data were segmented into five parts: gray matter, white matter, cerebrospinal fluid, skull bone, and head sculp. Segmentation was made using the SPM12 software package (the New Segmentation tool). The size of the finite elements did not exceed 2 mm. The values of electric conductivity coefficients for each of the above-mentioned biological tissues were taken from study [11]. The electrical field was calculated using the ANSYS package (ANSYS, United States). Details for the construction of an individual head model, as well as for the solution of the direct EEG problem, are given in the studies [12, 13].

The digitization of EEG-electrode positions for obtaining their coordinates in the MRT-image-related system was made using an NBS Eximia Nexstim device for navigational transcranial magnetic stimulation.

For each component determined, the EEG inverse problem was solved according to the *sLORETA* method [14]. The result of the solution of the inverse problem according to this method is the distribution of dipole moments over the entire brain volume that corresponds to the distribution of the potential on the head surface that is defined by the weight vector for a component with number i according to Eq. (1). The coordinates of maximum dipole moments were chosen as coordinates of the source.

To compare the data on the subjects with each other and with the published data on fMRI, we transformed the coordinates of EEG sources that were obtained taking into account the individual head geometry into the coordinates of the standardized atlas of the Montreal Neurological Institute (MNI) using the Normalize tool from the SPM12 software package.

RESULTS

Figure 1 shows the probabilities of the correct task recognition during the BCI performance that were averaged with respect to all sessions for each subject. For all subjects, the values exceeded the random level of recognition of three states (0.33). The wide distribution of the subjects with respect to the accuracy of recognition corresponds to our previous [15, 16] and published data [17]. The accuracy of BCI control was the same for healthy subjects and poststroke patients (Mann–Whitney test, $p = 0.64$), although the trend towards its decrease is noticeable in the patients. This is consistent with the data that we previously obtained [15, 16].

Components that are most frequently identified by the AMICA method. For detailed analysis, we found the independent components that occurred in more than 50% of all sessions among all subjects. The similarity of the components was assessed by the similarity of

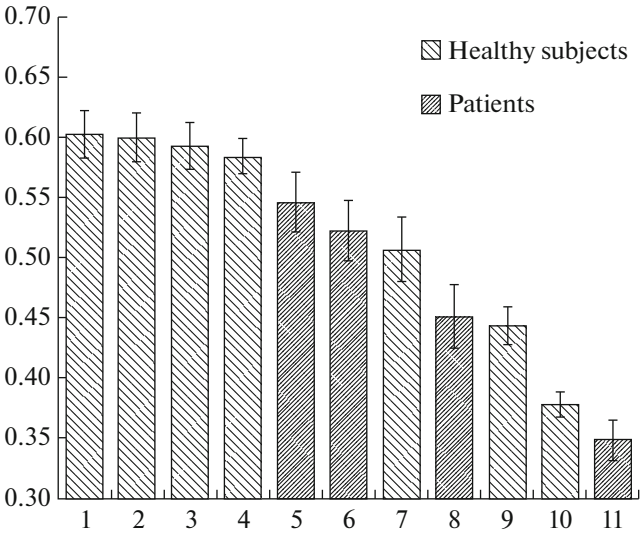

Fig. 1. The probability of the correct recognition of the performed tasks during BCI control that is averaged over all sessions for each subject and the standard error. The numbers of the subjects are shown on the abscise axis. The light columns correspond to the healthy subjects and the dark columns correspond to the patients.

their topographic maps. The number of components that met this selection criterion was five. An example of the selected components for one of the subjects is given in Fig. 2, where the spectral densities of their activity during the performance of the instructions, as well as the topographic maps that describe the electric potential distribution over the head surface, are shown.

The components were called according to the brain area in which the related sources were located: *SIL* (the primary somatosensory left cortex), *SIR* (the primary somatosensory right cortex), *PRC* (the precuneus), *PRM* (the premotor left cortex), and *SMA* (the supplementary motor area). The precuneus and supplementaty left and right motor areas are adjacent with each other and, as a rule, the relevant sources for the *PRC* and *SMA* components could not be located in the left or right brain. The component that corresponded to the source in the premotor right brain was identified two times less frequently than that for the left brain and was not included in the selected components.

Table 1 shows the frequencies of extraction of the selected components for the healthy subjects and poststroke patients. The *SIL* and *SIR* components were identified most frequently for all sessions and all subjects. These components were also regularly identified by other ICA methods and were previously described by us in detail [13, 15, 16, 18]. In those studies, they were designated as μ_1 and μ_2. The frequency of extraction of the components is somewhat lower for the patients than for the healthy subjects. Since it is these components that are the most significant for the

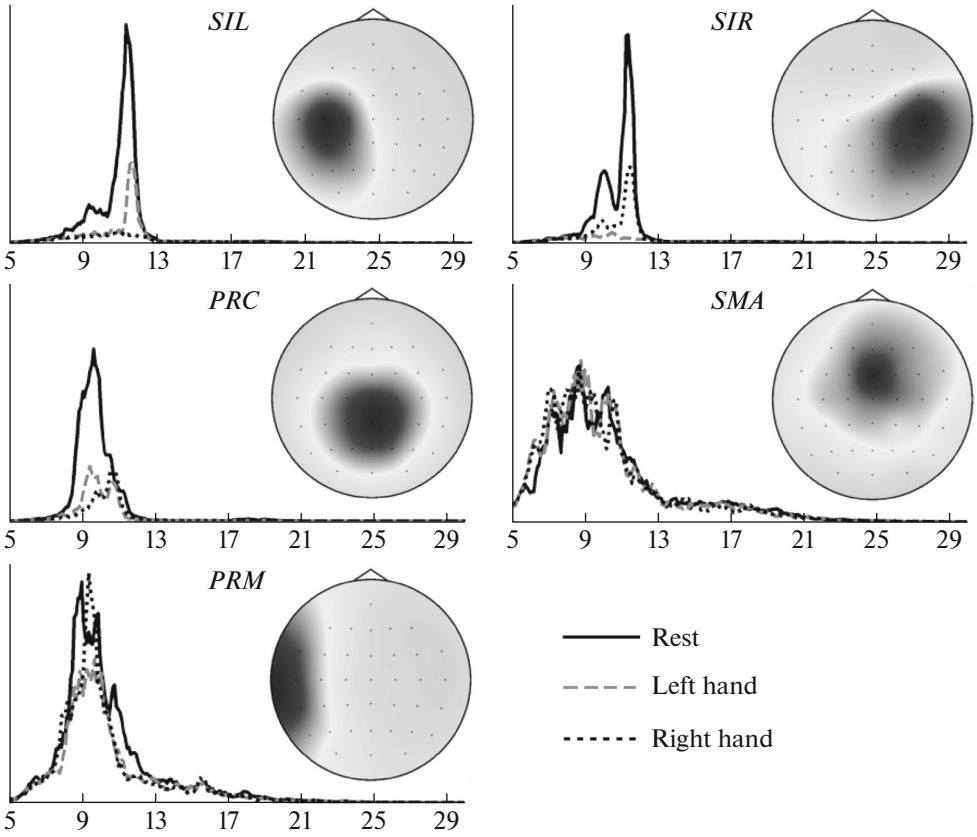

Fig. 2. The distribution of the potential over the head surface and the spectral densities of the power of activity for the most frequently occurring ICA components. An example of the components that were extracted in the final session for subject 2 (according to the numeration of the subjects in Fig. 1) is given. The darker the color on the topographic map, the higher is the contribution of the component to the signal on the respective electrode. The solid lines in the spectral density plots correspond to the state of relaxation, the dashed lines correspond to left hand motor imagery, and the dotted lines correspond to right hand motor imagery. The abscise axes indicate the frequency values in Hertz. The *SIL* notation corresponds to the source in the primary somatosensory left cortex, the *SIR* notation corresponds to the source in the primary somatosensory right cortex, *PRC* corresponds to the source in the precuneus, *SMA* corresponds to the source in the supplementary motor area, and *PRM* corresponds to the source in the premotor left brain.

recognition of EEG patterns during the performance of the instruction [13, 15, 16, 18], the decrease in the frequency of their extraction is in agreement with the trend towards a reduction in the accuracy of recognition of mental tasks performed by patients, as shown in Fig. 1.

When considering the spectral densities of activities of the selected components that are given in Fig. 2, one can see that the *SIL* and *SIR* components exhibit a well pronounced reaction of desynchronization in the α-band (8–13 Hz) during contralateral hand motor imagery. The *PRC* component exhibits a less pronounced desynchronization reaction that is the same for right and left hand motor imagery. For *PRM* and *SMA* components, the spectral density of activity does not depend on a task being performed.

The intensity of the reaction of desynchronization of the component during hand motor imagery can be assessed by the ratio of the power of its activity in the α-band during motor imagery to the power of its activity in the state of relaxation. The values of the degree of suppression of the rhythm that are averaged over all sessions are given in Table 1 for each patient and healthy subject. For the *SIL* and *SIR* components, the rhythm suppression is the highest during contralateral hand motor imagery. Its slight suppression is also observed for the ipsilateral hand. In contrast, we previously observed a slight increase in the μ-rhythm (the synchronization reaction) during ipsilateral hand motor imagery [12, 18]. The suppression of the μ-rhythm during contralateral hand motor imagery is expressed much less significantly in the patients than in the healthy subjects. This is another possible cause of a decrease in the accuracy of recognition of their mental states during the BCI control. The *PRC* component had a slight suppression of activity, which was the same during right and left hand motor imagery. Its increase was observed in the patients. The same was observed for the *PRM* component; in particular, the increase in the activity with respect to this component

Table 1. Characteristics of revealed EEG sources; the mean values and standard errors are shown

Characteristics of sources	*SIR*		*SIL*		*PRC*		*PRM*		*SMA*	
	healthy subjects	patients	healthy subjects	patients	healthy subjects	patients	healthy subjects	patients	healthy subjects	patients
Occurrence rate (% of sessions)	96	85	92	85	80	74	63	51	58	56
Level of suppression (left hand)	0.41 ± 0.03	0.91 ± 0.05	0.45 ± 0.04	0.86 ± 0.02	0.73 ± 0.04	1.23 ± 0.04	0.86 ± 0.05	1.37 ± 0.05	0.97 ± 0.02	0.95 ± 0.02
Level of suppression (right hand)	0.49 ± 0.02	0.81 ± 0.04	0.40 ± 0.06	0.76 ± 0.02	0.71 ± 0.05	1.48 ± 0.02	0.85 ± 0.01	1.70 ± 0.13	0.94 ± 0.02	1.02 ± 0.01
Fundamental frequency (rest), Hz	10.16 ± 0.18	9.54 ± 0.07	10.32 ± 0.02	9.55 ± 0.16	9.58 ± 0.04	9.36 ± 0.09	9.41 ± 0.00	9.21 ± 0.08	8.93 ± 0.11	9.02 ± 0.05
Fundamental frequency (left hand), Hz	9.27 ± 0.03	9.55 ± 0.09	10.05 ± 0.05	9.57 ± 0.18	9.60 ± 0.06	9.34 ± 0.06	9.36 ± 0.10	9.29 ± 0.33	8.88 ± 0.08	9.05 ± 0.06
Fundamental frequency (right hand), Hz	9.85 ± 0.15	9.45 ± 0.05	9.49 ± 0.05	9.63 ± 0.16	9.67 ± 0.09	9.36 ± 0.11	9.28 ± 0.04	9.46 ± 0.23	8.79 ± 0.08	9.22 ± 0.05
Degree of the frequency peak (rest)	0.72 ± 0.01	0.38 ± 0.01	0.82 ± 0.03	0.37 ± 0.02	0.58 ± 0.02	0.39 ± 0.01	0.44 ± 0.08	0.35 ± 0.03	0.37 ± 0.01	0.32 ± 0.01
Degree of the frequency peak (left hand), Hz	0.37 ± 0.01	0.41 ± 0.02	0.52 ± 0.01	0.36 ± 0.02	0.52 ± 0.02	0.43 ± 0.02	0.46 ± 0.03	0.38 ± 0.02	0.35 ± 0.02	0.33 ± 0.02
Degree of the frequency peak (right hand), Hz	0.47 ± 0.01	0.40 ± 0.01	0.38 ± 0.03	0.35 ± 0.02	0.53 ± 0.04	0.46 ± 0.02	0.47 ± 0.15	0.41 ± 0.03	0.34 ± 0.01	0.35 ± 0.03
Coordinates of the source according to EEG (MNI)	28; –32; 54		–31; –33; 53		–1; –51; 57		–34; –1; 45		–6; –21; 75	
Coordinates of the fMRI source (MNI)	39; –28; 49		–39; 28; 49		–15; –58; 61 15; –61; 61		–24; –4; 58		–3; 8; 55 6; 8; 58	

was rather significant for the patients. For the *SMA* component, the activity remained almost the same during motor imagery.

In Fig. 2, the peak spectral density is more diffused towards an increase in the signal strength in the β-band for the activity of the *SMA* component than in the other components. This is in line with the data of [19], in which a higher intensity of the β-activity in *SMA* according to the corticogram is shown. For the other components, the peak spectral density is more pronounced in the state of rest and its intensity and peak frequency decrease during motor imagery. The degree of the peak can be assessed by the ratio of the peak power spectrum to the residual power spectrum in the α-band, where the peak power is defined as activity power in the interval with a width of 1 Hz and with the center in the peak frequency. Accordingly, this range was excluded from the α-band for calculating the residual power. It is easy to see that the value of the peak degree will be 0.25 when the spectral density is evenly distributed in the α-range, i.e., when the peak is absent. If this value is exceeded, one can state the presence of the peak.

Table 1 shows the values of the peak degree that are averaged over all sessions, individually for the healthy subjects and for the patients. As in the subject for which the data are shown in Fig. 2, the degree of the peak in the healthy subjects is, on average, the highest for the *SIL*, *SIR*, and *PRC* components. Their peaks were less pronounced when the suppression of the μ-rhythm was higher. In the patients, the degree of the peaks was much less dependent on a mental task being performed. Their lowest degree in both the healthy subjects and the patients was observed for the *SMA* component.

Table 1 also shows the values of peak frequencies, i.e., the frequencies that correspond to the maximum spectral density in the α-band, which are averaged over all sessions individually for the patients and subjects. All the frequency values actually correspond to the low-frequency α-range (less than 10 Hz); the peaks corresponded to the high-frequency α-band for the state of rest in the healthy patients. During motor imagery, these peaks shifted towards lower frequencies.

Location of EEG sources. The sources of electrophysiological brain activity were located according to the data on the final day of experiments for each subject, when the positions of electrodes were accurately measured in the MRT coordinate system (see "Methods"). For the *SIR* and *SIL* components, the peak density of current that was found using the *sLORETA* method was determined for all subjects near the lower boundary of the central sulcus, where Brodmann area 3a, which is responsible for proprioceptive hand sensibility, is located [20]. This is in line with the results that were previously obtained for these components by searching for the optimal position of a single current dipole, which best corresponds to the topographic maps of these components [12, 13, 18].

Figures 3 and 4 present the data on the location of sources in the MNI space that were averaged with respect to all sessions on the final day for all subjects. The position of each source is presented by an ellipsoid that includes 70% of all location points that were found for all sessions and all subjects. The size of the ellipsoids defines the accuracy of location of sources. For instance, for the *SIR* and *SIL* components, the semi-axes of the ellipsoids are (11, 7, 4) mm and (10, 7, 6) mm. The centers of the ellipsoids correspond to the mean coordinates of the sources, which are given in Table 1.

Figure 4 compares the locations of the *SIR* and *SIL* sources that were determined according to the individual and standard head geometry in the MNI atlas. One can see that the solution of the EEG inverse problem without consideration of the individual head geometry yields the forward and upward shift of the sources by 35 mm. Approximately the same shift of these sources was previously observed by us when they were located by searching for the positions of a single current dipole, which provides the best approximation of the topographic maps of the relevant components [18]. Therefore, the solution of the EEG inverse problem without consideration of the individual geometry of the brain and its covers may lead to a significant error.

DISCUSSION

Previously [12, 13, 18], we have already described two symmetrical EEG sources for healthy subjects, which are located at the bottom of the central sulcus in Brodmann area 3a, responsible for proprioceptive hand sensibility, in the primary somatosensory cortex [20]. These sources exhibit the reaction of the μ-rhythm desynchronization during contralateral hand motor imagery; this reaction corresponds to the activation in the area of hand representation, which is also observed during the performance and observation of movements [21, 22]. They are regularly extracted by all independent component methods during the analysis of EEG records that were obtained when BCIs based on motor imagery were studied [7, 12, 18, 23]. The μ-rhythm in the somatosensory area was characterized by a lower frequency in the studied poststroke patients than in the healthy subjects; it had a poorly pronounced peak in all mental states and was only slightly suppressed during contralateral hand motor imagery.

The rhythm in the α-band was also characterized by a low frequency with a poorly pronounced peak in the precuneus and premotor area; however, unlike in the healthy subjects, this rhythm increased, i.e., was synchronized, during motor imagery. If we follow the general idea, according to which the increase in the rhythm of the α-band reflects a decrease in brain

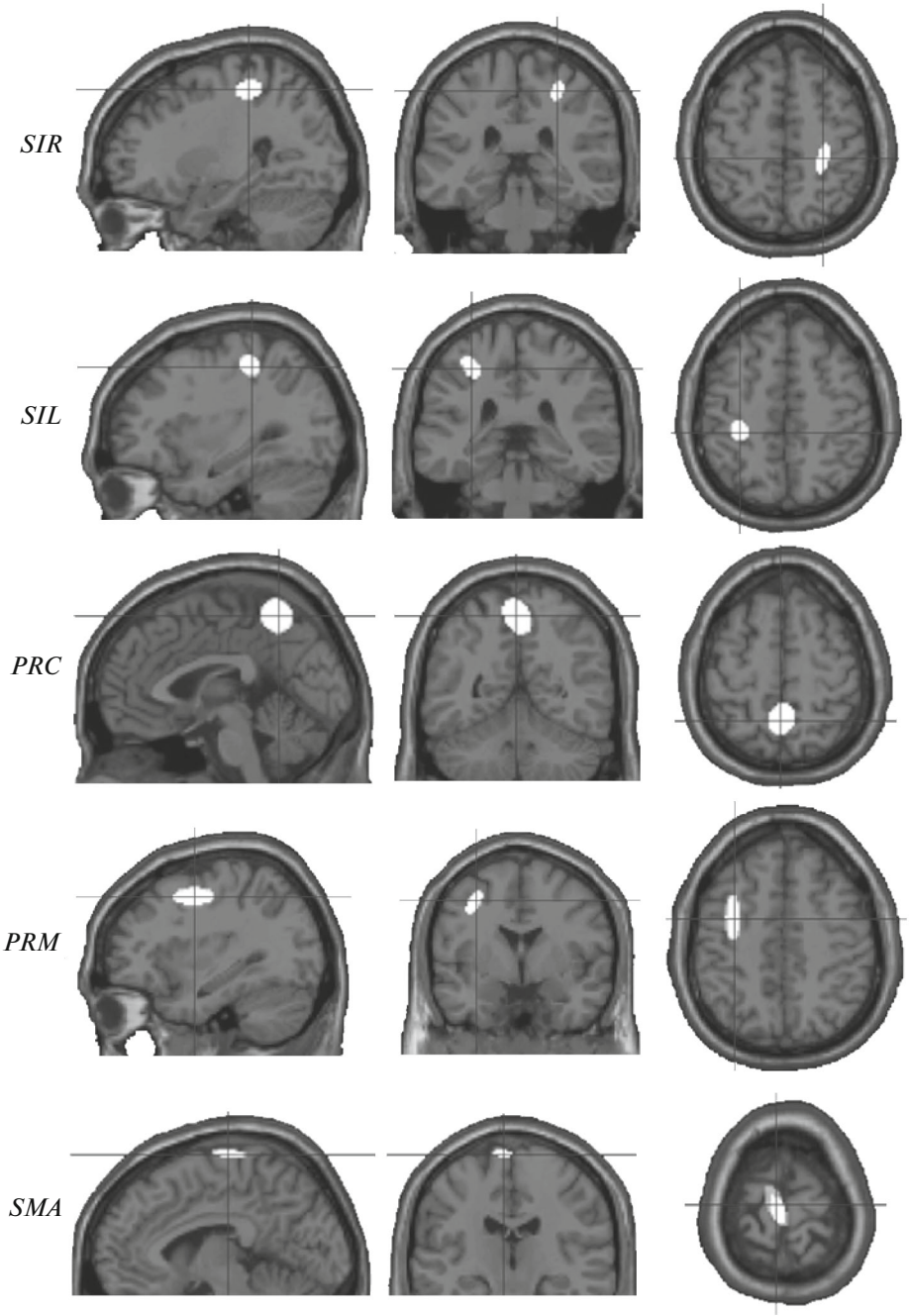

Fig. 3. The areas that characterize the range of locations of sources for components of each type that were obtained with respect to all subjects. The centers of white ellipses show the coordinates of the sources that were averaged with respect to all subjects, while the scatter of individual coordinates is defined by the boundaries of the ellipses. See the notations in Fig. 2.

activity, it can be assumed that the activity decreases in these areas during motor imagery in the patients, unlike the healthy subjects, in which it increases in this case. This assumption should be tested in additional experiments using fMRI. In the supplementary motor area, the rhythm in the α-band was almost completely independent from the task being performed with respect to all parameters for both healthy subjects and poststroke patients.

The most complete description of brain activity during motor imagery was obtained using fMRI. The metaanalysis that was performed in survey [24] showed that different studies on motor imagery regularly mention the activation of 34 brain areas. The activation of 28 of these areas was found in the study [8] during the motor imagery-based BCI control. Among the cortical areas, which are almost always activated during hand motor imagery, the study [24]

Fig. 4. Comparison of locations of *SIR* and *SIL* components that were found according to the individual head models and standard head model. As in Fig. 3, the average coordinates of sources (the centers of white ellipses) and their dispersion (the boundaries of the ellipses) are shown. When the individual head model is used for each subject, they are located at the bottom of the central sulcus (rear position in the presented brain slice; their location corresponds to the *SIR* and *SIL* components in Fig. 3). When the standard head model is used, their coordinates significantly shift forward (the frontal position in the presented brain slice).

mentions the inferior frontal sulcus, premotor area, middle frontal gyrus, supplementary motor area, insula, cingulate gyrus, superior and inferior parietal lobes, supramarginal gyrus, postcentral gyrus, and precuneus. Among these brain areas, which are activated according to the fMRI, it is the supplementary motor area, precuneus, and premotor area that contain the EEG sources that were described in the previous section.

In addition to the fact that the EEG sources and fMRI foci that were located in the same brain areas are identified with different frequencies, their location in these areas is also different. Table 1 compares the coordinates of the EEG sources with the coordinates of the fMRI foci that were determined in [8] for healthy subjects. For the *PRC* and *SMA* components, the coordinates of the fMRI foci are given separately for the left and right hemispheres, unlike the respective EEG sources, the division of which with respect to the right and left hemispheres was difficult due to their proximity.

Table 1 shows that the locations of the EEG sources and respective fMRI foci are approximately 1 cm different. For instance, the sources of the μ-rhythm that were located in the central sulcus were deeper than the respective foci of hemodynamic activity. The same mutual position of these sources was previously found by us [12, 18] during the location of the sources by optimizing the position of a single dipole. The difference in the locations of EEG sources and fMRI foci seems to be natural rather than being the consequence of the inaccuracy of their location. For instance, during the study of responses to electric hand stimulation under the conditions when the locations of the sources of electrophysiological activity and focus of hemodynamic activity in response to the stimulation could be determined most accurately, their difference was up to 25 mm [25–27]. This is possibly due to the fact that EEG and fMRI are activated by different processes: EEG is a result of postsynaptic neuron activity, while the response that is observed in the case of fMRI is a result of the change in the concentrations of oxidized and nonoxidized hemoglobin due to the most costly energy processes. Since the relationship between postsynaptic neuron activity and the value of the hemodynamic response is complex [28], the brain areas where these two reactions to the same activity are most highly pronounced may be different.

There is much evidence of inverse correlation between the amplitude of the rhythm in the α-band and the intensity of hemodynamic activity. Our experiments confirmed this general concept. For healthy subjects, the hemodynamic activity increased [8] and the rhythm in the α-band was suppressed in all the investigated brain areas during motor imagery. This pattern was particularly pronounced in the primary somatosensory cortex (Table 1) and was expressed in the suppression of the high-frequency component of the μ-rhythm. For all the other sources, the suppression of the α-rhythm was low and the rhythm had a low frequency and a poorly pronounced peak. This is in agreement with the prevailing opinion that the low-frequency rhythm is topographically more widespread over the cortical surface and less specific with respect to manifestations and is possibly associated with the requirement of a certain level of general attention in solving a wide variety of problems. In contrast, the rhythm with a higher frequency in the α-band is topographically less distributed over the cortex and its changes are related to the processing of semantic and sensory information [29–31].

The sources of activity in the α-band are pronounced most frequently in five of the considered brain areas during the motor imagery-based BCI control. These sources are episodically found for much a greater number of brain areas [16]. It is known that almost the same areas are activated during the performance, imagery, and observation of movements [32]. According to Jeannerod [33], this is due to the fact that the performance of all these mental tasks requires the internal movement presentation, while the imagery of movement is the prolongation of internal presentation due to the multiple rehearsal of this movement in the working memory during motor command inhibition [32, 34]. The internal movement presentation requires the involvement of a large number of brain areas, since it is a difficult cognitive task that is solved on the basis

of the performance of different kinds of sensomotor transformations: first, the transformation of the goal of movement into the motor command that provides its achievement; second, the transformation of the command into the prediction of sensory signals that will be generated as a result of its performance [35, 36]. The first transformation is performed on the basis of the so called inverse internal neural model, while the second is performed on the basis of the direct neural model [35].

The inverse model receives the current sensory signal, which sets the parameters of the object related to the movement goal (including its position, size, shape, etc.) and yields a motor command that provides the required object manipulation. The direct model receives the efferent copy of the motor command and the model output is an expected sensory signal (*corollary discharge*) which will be appear as a result of the command performance. The necessity of prediction of a sensory signal, depending on intended movement, was comprehensively described for the first time by Poincare as far back as 100 years ago [37]. Since changes in the sensory flow are related both with human self-motions, provided the constant external environment, and with changes in the surrounding medium, it is essential to extract those signals from the flow which are related with changes in the medium. This can be achieved only by predicting changes in sensory signals in the constant medium as a result of self-motions using the direct model. The necessity of predicting changes in a sensory signal, depending on self-movements, is most evident from the example of eye movements [38, 39]. Although it has not been definitely determined where these models are located, how they interact with each other, and whether they actually exist [35], the above-mentioned theoretical considerations indicate the necessity of their existence quite convincingly.

The simplest illustration of the above-mentioned concepts of interaction of internal models is the hypothesis of the role of the primary somatosensory area during the imagery, performance, and observation of movements that we proposed in study [40]. According to this hypothesis, this area receives a predicted proprioceptive signal on the performance of imaginary movement from the premotor area; i.e., it receives a signal from the output of the direct model. This signal is compared with a real peripheral proprioceptive signal in the primary somatosensory area. According to their mismatch , the command for muscle activation is formed in the primary motor area. To achieve a more exact perception of the peripheral proprioceptive signal, the primary somatosensory area is set in the activation regime, which is accompanied by a decrease in the amplitude of the high-frequency μ-rhythm. During the imagery and observation of movements, the motor command is blocked, presumably by the supplementary motor area [41, 42].

More complex loops of interaction of frontal and parietal brain areas during the performance and observation of movements are considered in the study [36]; however, these loops involve the brain areas that were not included in the group of areas in which the sources of electrophysiological activity that were considered by this study are regularly extracted.

CONCLUSIONS

This study is an extension of previous investigations of EEGs during motor imagery by healthy subjects, as well as their comparison with the fMRI foci [12, 13, 18]. Only two symmetrical sources in the primary somatosensory cortex were previously discussed. This study also adds three more sources to them: the premotor area, precuneus, and supplementary motor area. It was found that the highest suppression of the μ-rhythm during motor imagery is observed in the primary somatosensory area; this suppression relates to the high-frequency rhythm in the α-band that has a sharp peak in the spectrogram. The other areas had a low-frequency rhythm with a poorly pronounced peak in the α-band. The functioning of EEG sources was studied in a small group of poststroke patients with the subcortical location of the damage. The results of the study showed that the characteristics of the sources fundamentally changed in the patients from this group. First, the high-frequency μ-rhythm decreased in the primary somatosensory cortex in the state of rest and the level of its suppression during motor imagery decreased. Second, unlike in the healthy subjects, the sources in the premotor area and precuneus in the patients exhibited an increase in the amplitude of the rhythm in the α-band during motor imagery. Bearing in mind that there is an inverse correlation between the amplitude of the rhythm and hemodynamic brain activity, one can assume that these areas decrease their activity during motor imagery. The test of this assumption is the purpose of further studies.

ACKNOWLEDGMENTS

This study was supported by the Russian Foundation for Basic Research, project nos. 16-29-08206 ofi_m and 16-29-08247 ofi_m.

REFERENCES

1. Kotov, S.V., Turbina, L.G., Bobrov, P.D., Frolov, A.A., Pavlova, O.G., Kurganskaya, M.E., and Biryukova, E.V., Rehabilitation of stroke patients with a bioengineered “brain–computer interface with exoskeleton” system, *Neurosci. Behav. Physiol.*, 2016, vol. 46, no. 5, p. 518.
2. Frolov, A.A., Mokienko, O.A., Lyukmanov, R.Kh., Chernikova, L.A., Kotov, S.V., Turbina, L.G., Bobrov, P.D., Biryukova, E.V., Kondur, A.A., Ivanova, G.E., Staritsyn, A.N., Bushkova, Yu.V., Dzhalagoniya, I.Z., Kurganskaya, M.E., Pavlova, O.G.,

et al., Preliminary results of a controlled study of BCI–exoskeleton technology efficacy in patients with post-stroke arm paresis, *Bull. Russ. State Med. Univ.*, 2016, no. 2, p. 16.

3. Ang, K.K., Chua, K.S., Phua, K.S., et al., A randomized controlled trial of EEG-based motor imagery brain–computer interface robotic rehabilitation for stroke, *Clin EEG Neurosci.*, 2015, vol. 46, no. 4, p. 310.
4. Ramos-Murguialday, A., Broetz, D., Rea, M., et al., Brain–machine interface in chronic stroke rehabilitation: a controlled study, *Ann Neurol.*, 2013, vol. 74, no. 1, p. 100.
5. Delorme, A., Palmer, J., Onton, J., et al., Independent EEG sources are dipolar, *PloS One*, 2012, vol. 7, no. 2, e30135.
6. Onton, J., Westerfield, M., Townsend, J., and Makeig, S., Imaging human EEG dynamics using independent component analysis, *Neurosci. Biobehav. Rev.*, 2006, vol. 30, no. 6, p. 808.
7. Kachenoura, A., Albera, L., Senhadji, L., Comon, P., ICA: a potential tool for BCI systems, *IEEE Signal Process. Mag.*, 2008, vol. 25, no. 1, p. 57.
8. Frolov, A.A., Husek, D., Silchenko, A., et al., The changes in the hemodynamic activity of the brain during motor imagery training with the use of brain–computer interface, *Hum. Physiol.*, 2016, vol. 42, no. 1, p. 1.
9. Bobrov, P.D., Korshakov, A.V., Roshchin, V.Yu., and Frolov, A.A., Bayesian approach to the implementation of the brain–computer interface based on the imaged movements, *Zh. Vyssh. Nervn. Deyat. im. I.P. Pavlova*, 2012, vol. 62, no. 1, p. 89.
10. Palmer, J.A., Kreutz-Delgado, K., and Makeig, S., *AMICA: An Adaptive Mixture of Independent Component Analyzers with Shared Components. Technical Report*, San Diego, CA: Swartz Center Comput. Neurosci., 2011.
11. Kim, T.S., Zhou, Y., Kim, S., and Singh, M., EEG distributed source imaging with a realistic finite-element head model, *IEEE Trans. Nucl. Sci.*, 2002, vol. 49, no. 3, p. 745.
12. Frolov, A., Bobrov, P., Mokienko, O., et al., Sources of EEG activity most relevant to performance of brain-computer interface based on motor imagery, *Neural Network World*, 2012, vol. 22, no. 1, p. 21.
13. Frolov, A.A., Husek, D., Bobrov, P.D., et al., Localization of brain electrical activity sources and hemodynamic activity foci during motor imagery, *Hum. Physiol.*, 2014, vol. 40, no. 3, p. 273.
14. Pascual-Marqui, R.D., Standardized low-resolution brain electromagnetic tomography (sLORETA): technical, *Methods Find. Exp. Clin. Pharmacol.*, 2002, vol. 24, p. 5.
15. Frolov, A.A., Biryukova, E.V., Bobrov, P.D., et al., Principles of neurorehabilitation based on the brain-computer interface and biologically adequate control of the exoskeleton, *Hum. Physiol.*, 2013, vol. 39, no. 2, p. 196.
16. Frolov, A.A., Husek, D., Biryukova, E.V., et al., Principles of motor recovery in post-stroke patients using hand exoskeleton controlled by the brain-computer interface based on motor imagery, *Neural Network World*, 2017, vol. 27, no. 1, p. 107.
17. Pfurtscheller, G. and Neuper, C., Motor imagery and direct brain-computer communication, *Proc. IEEE*, 2001, vol. 89, no. 7, p. 1123.
18. Bobrov, P.D., Isaev, M.R., Korshakov, A.V., et al., Sources of electrophysiological and foci of hemodynamic brain activity most relevant for controlling a hybrid brain computer interface based on classification of EEG patterns and near-infrared spectrography signals during motor imagery, *Hum. Physiol.*, 2016, vol. 42, no. 3, p. 241.
19. Ohara, S., Ikeda, A., Kunieda, T., et al., Movement-related changes of electrocorticographic activity in human supplementary motor area proper, *Brain*, 2000, vol. 123, p. 1203.
20. Kaukoranta, E., Hamalainen, M., Sarvas, J., and Hari, R., Mixed and sensory nerve stimulations activate different cytoarchitectonic areas in the human primary somatosensory cortex SI, *Exp. Brain Res.*, 1986, vol. 63, p. 60.
21. Cochin, S., Barthelemy, C., Roux, S., and Martineau, J., Observation and execution of movement: similarities demonstrated by quantified electroencephalography, *Eur. J. Neurosci.*, 1999, vol. 11, no. 5, p. 1839.
22. Francuz, P. and Zapała, D., The suppression of the μ rhythm during the creation of imagery representation of movement, *Neurosci. Lett.*, 2011, vol. 495, no. 1, p. 39.
23. Ball, K., Bigdely-Shamlo, N., Mullen, T., and Robbins, K., PWC-ICA: a method for stationary ordered blind source separation with application to EEG, *Comput. Intell. Neurosci.*, 2016, vol. 2016, no. 9754813.
24. Hetu, S., Grégoire, M., Saimpont, A., et al., The neural network of motor imagery: an ALE meta-analysis, *Neurosci. Biobehav. Rev.*, 2013, vol. 37, no. 5, p. 930.
25. Del Grattaf, C., Della Penna, S., Ferretti, A., et al., Topographic organization of the human primary and secondary somatosensory cortices: comparison of fMRI and MEG findings, *NeuroImage*, 2002, vol. 17, no. 3, p. 1373.
26. Christmann, C., Ruf, M., Braus, D.F., and Flor, H., Simultaneous electroencephalography and functional magnetic resonance imaging of primary and secondary somatosensory cortex in humans after electric stimulation, *Neurosci. Lett.*, 2002, vol. 333, p. 69.
27. Thees, S., Blabkenburg, F., Taskin, B., et al., Dipole source localization and fMRI of simultaneously recorded data applied to somatosensory categorization, *NeuroImage*, 2003, vol. 18, p. 707.
28. Goebel, R. and Esposito, F., The added values of EEG-fMRI in imaging neurosience, in *EEG-fMRI. Physiological Basis, Technique, and Applications*, Mulert, C. and Lemieux, L., Eds., Berlin: Springer, 2009, p. 97.
29. Klimesch, W., EEG alpha and theta oscillations reflect cognitive and memory performance: a review and analysis, *Brain Res. Rev.*, 1999, vol. 29, nos. 2–3, p. 169.
30. Klimesch, W., Alpha-band oscillations, attention, and controlled access to stored information, *Trends Cognit. Sci.*, 2012, vol. 16, no. 12, p. 606.
31. Pfurtscheller, G. and Lopes da Silva, F.H., Event-related EEG/MEG synchronization and desynchroni-

zation: basic principles, *Clin. Neurophysiol.*, 1999, vol. 110, no. 11, p. 1842.

32. Decety, J. and Grèzes, J., Neural mechanisms subserving the perception of human actions, *Trends Cognit. Sci.*, 1999, vol. 3, no. 5, p. 172.
33. Jeannerod, M., The representing brain: Neural correlates of motor intention and imagery, *Behav. Brain Sci.*, 1994, vol. 17, no. 2, p. 187.
34. Guillot, A., Di Rienzo, F., and MacIntyre, T., Imagining is not doing but involves specific motor commands: a review of experimental data related to motor inhibition, *Front. Hum. Neurosci.*, 2012, vol. 6, art. ID 247.
35. Wolpert, D.M., Ghahramani, Z., and Jordan, M.I., An internal model for sensorimotor integration, *Science*, 1995, vol. 269, no. 5232, p. 1880.
36. Rizzolatti, G., Cattaneo, L., Fabbri-Destro, M., and Rozzi, S., Cortical mechanisms underlying the organization of goal-directed actions and mirror neuron-based action understanding, *Physiol. Rev.*, 2014, vol. 94, no. 2, p. 655.
37. Poincaré, H., *La Science et l'Hypothèse, Paris: Flammarion, 1902; La Valeur de la Science, Paris: Flammarion, 1905; Science et Méthode, Paris: Flammarion, 1908; Dernières Pensées*, Paris: Flammarion, 1913.
38. Von Holst, E., Relations between the central nervous system and the peripheral organs, *Br. J. Anim. Behav.*, 1954, vol. 2, p. 89.
39. Sperry, R.W., Neural basis of spontaneous optokinetic responses produced by visual inversion, *J. Comp. Physiol. Psychol.*, 1950, vol. 43, p. 482.
40. Frolov, A.A., Fedotova, I.R., Gusek, D., and Bobrov, P.D., Rhythmic brain activity and brain-computer interface based on motor imagery, *Usp. Fiz. Nauk*, 2017, vol. 48, no. 3, p. 72.
41. Kasess, C.H., Windischberger, C., Cunnington, R., et al., The suppressive influence of SMA on M1 in motor imagery revealed by fMRI and dynamic causal modeling, *NeuroImage*, 2008, vol. 40, p. 828.
42. Hanakawa, T., Dimyan, M.A., and Hallett, M., Motor planning, imagery, and execution in the distributed motor network: a time course study with functional MRI, *Cereb. Cortex*, 2008, vol. 18, p. 2775.

Translated by D. Zabolotny